Gravitational instability of miscible fluids in a Hele-Shaw cell

J. Martin,[a] N. Rakotomalala, and D. Salin
Laboratoire Fluides Automatique et Systèmes Thermiques, Universités P. et M. Curie and Paris Sud, C.N.R.S. (UMR 7608), Bâtiment 502, Campus Universitaire, 91405 Orsay Cedex, France

(Received 28 February 2001; accepted 30 October 2001)

We revisit the Rayleigh–Taylor instability when the two fluids are miscible and in the geometry of a Hele-Shaw cell. We provide analytical dispersion relations for the particular cases of either a sharp front between the two fluids or of a uniform density gradient stratification and for various fluid flow models, including an unbounded geometry, a two-dimensional gap-averaged Navier–Stokes–Darcy equation, and an effective porous medium. The results are compared to three-dimensional lattice BGK simulations, based on which the relevance of the various models in different wavelength regimes is discussed. © *2002 American Institute of Physics.* [DOI: 10.1063/1.1431245]

When a denser fluid rests on top of a lighter one in a gravitational field, the interface between the fluids is unstable. This so-called Rayleigh–Taylor (RT) instability[1] has been extensively studied for the case of two immiscible fluids. There, viscosity and interfacial tension act as stabilizing factors. The instability has also been analyzed in the case of miscible fluids in porous media geometries.[2] In miscible fluids, the stabilizing role of interfacial tension is played by molecular diffusion. A reduced density contrast, as a result of a mixing zone between the fluids, also acts to mitigate the instability.[3,4] The present Brief Communication addresses the RT instability between miscible fluids in a Hele-Shaw cell. This geometry, consisting of two parallel plates separated by a small gap of thickness h, is routinely used in laboratory experiments. Our objective is to compare the linear stability predictions of various models describing miscible flow in the Hele-Shaw cell, with three-dimensional (3D) lattice Bhatnagar–Gross–Krook (BGK) simulations[5] to discuss the relevance of the various models. In particular, we focus on the use of the averaged two-dimensional (2D) Navier–Stokes–Darcy (NSD) equation, which allows us to unify the linear stability analyses in unbounded geometries, porous media and Hele-Shaw cells. Based on the RT problem in unbounded geometries[4] we define a miscible Rayleigh–Taylor (MRT) length L, involving buoyancy, and viscous and molecular diffusion, to normalize length scales. The Darcy model for the Hele-Shaw cell description is valid when the cell gap is small compared to this characteristic length ($h \ll L$), whereas the unbounded geometry case is obtained in the opposite limit ($h \gg L$). Use of the NSD approach allows us to recover these two limits, and is shown to also give a good approximation in the intermediate range of cell thicknesses. Results for the analytical dispersion relations are given for two limiting cases involving a uniform density gradient stratification or a sharp front between the two fluids. This could find applications in chemical wave fronts, where autocatalytic reactions create a mixing zone of a very small extension compared to the characteristic length.[6]

Consider a base state consisting of a mixture of two miscible fluids of concentration $C(z)$ varying along the upward oriented vertical coordinate z. This gives rise to a corresponding density profile $\rho_1(z)=\rho_0+\Delta\rho(C(z)-0.5)$, where $\Delta\rho$ and ρ_0 denote the difference and the average of the densities of the two miscible fluids, respectively. The kinematic viscosity ν and the molecular diffusivity D are assumed to be constant in the mixture. In the case of laterally unbounded geometries, a linear stability analysis of such a base state was obtained by Batchelor and Nitsche,[4] using a convection-diffusion equation (CDE), the Navier–Stokes equations under the Boussinesq approximation (the density variations affect only the gravitational force), and a quasi-static base state approximation. In the absence of vertical boundaries, the Fourier components of the disturbance with respect to the horizontal coordinate x are independent. Therefore for a normal mode of wave vector k in the horizontal direction and a corresponding growth rate $\sigma(k)$, the vertical velocity in the perturbed state is $w(x,z,t)=W(z)e^{\sigma t+ikx}$, with analogous expressions for the density, pressure, and horizontal velocity. After calculations one finds that the vertical disturbance $W(z)$ obeys the following equation:

$$(\sigma/D+k^2-d_{ZZ})(\sigma/\nu+k^2-d_{ZZ})(k^2-d_{ZZ})W(z) = (gk^2/D\nu\rho_0)\,\Delta\rho(dC/dz)\,W(z), \quad (1)$$

where g is the gravity acceleration. For a given concentration profile $C(z)$, the dispersion relation $\sigma(k)$ can be obtained by various methods, including matched asymptotic expansions for the various regimes of the wave number. Taking the commonly used S-shape stratification of width e,

$$C(z)=\tfrac{1}{2}\,\mathrm{Erfc}(z/e), \quad (2)$$

allows us to treat uniformly the steplike density profile ($e \to 0$) and the uniform density gradient stratification ($e \to \infty$) cases. To convert Eq. (1) to dimensionless notation, we choose the characteristic length and time as the following:

$$L=(2\rho_0\nu D/\Delta\rho g)^{1/3} \quad \text{and} \quad T=L^2/\sqrt{\nu D}, \quad (3)$$

the selection of which emphasizes the symmetric role played by viscous and molecular diffusions. We note that for classi-

[a]Author to whom correspondence should be addressed. Electronic mail: martin@fast.u-psud.fr

cal fluids, the MRT length, L, will vary typically between 100 μm and 1 mm. This leads to dimensionless wave vector $q=kL$ and growth rate $n=\sigma T$, based on which Eq. (1) becomes

$$(q_D^2-d_{ZZ})(q_\nu^2-d_{ZZ})(q^2-d_{ZZ})W(Z)=2q^2(dC/dZ)\,W(Z). \tag{4}$$

Here, $Z=z/L$ and

$$q_D^2=q^2+n\sqrt{S_C} \quad \text{and} \quad q_\nu^2=q^2+n/\sqrt{S_C}, \tag{5}$$

where $S_C=\nu/D$ is the Schmidt number. We point out that the normalized cutoff wave vector q_C of the neutral mode ($n=0$) is independent of S_C. Two cases of Eq. (4) can be solved analytically, the steplike base state ($e=0$) and the case of a uniform density gradient.[4]

The step case yields an analytical dispersion relation[4,7] given by

$$q_\nu q_D(q_\nu+q_D)(q_\nu+q)(q+q_D)=q(q_\nu+q_D+q). \tag{6}$$

For the case of a uniform density gradient, the dispersion relation was established in Ref. 4. In the case of a S-shape profile, the latter is also obtained in the limit of large normalized width, $b=(e/L)\gg 1$. Identifying in this limit the uniform gradient with $\Delta\rho(dC/dz)(z=0)=(\Delta\rho/\sqrt{\pi}e)$, one finds

$$q_\nu^2 q_D^2=2/\sqrt{\pi}b\,. \tag{7}$$

The general case requires solution of the full dispersion relation [Eq. (4)]. We computed the eigenvalue problem using a numerical method for the case of a finite width. Results for $b=10$ and for $S_C=500$ and 1000, are plotted in the inset of Fig. 1. Also shown by open circles are corresponding 2D results from lattice BGK simulations[5] performed at $S_C=500$. The latter are in good agreement with the linear stability analysis. A description of the simulations will be briefly described in a later section. Comparison of the two curves shows that the maximum growth rate does not vary drastically with the Schmidt number, in the range of typical fluid Schmidt numbers. For completeness, we also note that the cutoff wave vector $q_C\sim 0.53$ is lower than the corresponding values of $q_{C,0}\sim 0.72$ and $q_{C,\infty}\sim 0.58$ obtained from Eqs. (6) and (7) corresponding to the two asymptotic regimes ($b=0$ and $b\to\infty$). The range of validity of the latter two regimes can be assessed in Fig. 1, which shows the cutoff wave vector q_C plotted versus $(1/b)^{1/4}$ (crosses). The dashed lines correspond to the zero width and uniform gradient limits, $q_{C,0}=(3/8)^{1/3}$ and $q_{C,\infty}=(2/\sqrt{\pi}b)^{1/4}$, respectively, which are expected to be recovered in the respective limits $b\ll 1$ and $b\gg 1$. Figure 1 shows that in practice, these two limits hold for $b<0.5$ and $b>20$, respectively. An empirical fit (full line) of the numerical data is also given to describe the crossover between the two regimes.

Describing the flow in a Hele-Shaw cell requires averaging the Navier–Stokes equations along the gap of the cell. In this paper, we will consider two different models.

Model 1. Averaging the assumed parabolic profile across the gap has led to the following 2D NSD equation:[8]

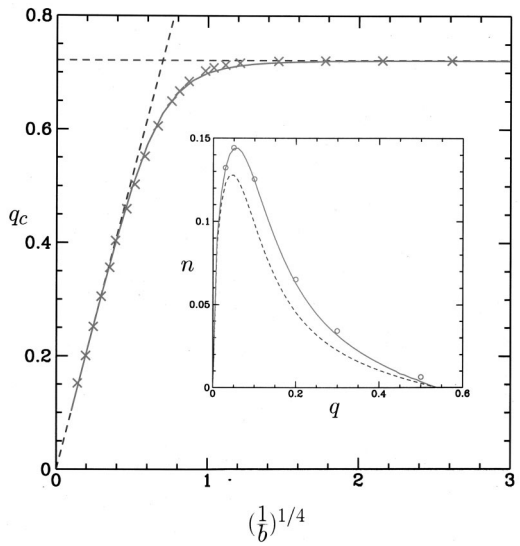

FIG. 1. Plot of the normalized cutoff wave vector, $q_C=k_CL$ vs $(1/b)^{1/4}$, for the RT instability. Here, $b=e/L$ is the normalized mixing width, using $L=(2\rho_0\nu D/\Delta\rho g)^{1/3}$. The results (crosses) are numerical solutions of the eigenvalue problem, in the case of unbounded fluids [Eqs. (4) and (5)]. The dashed lines correspond to the limits of step concentration profile ($b=0$), where $q_{C,0}=(3/8)^{1/3}$, and that of a constant gradient, where $q_{C,\infty}=(2/\sqrt{\pi b})^{1/4}$. The full line curve is a fit to the data using $q_C=[1/[(q_{C,0})^{-5}+(q_{C,\infty})^{-5}]]^{1/5}$. The inset displays the normalized dispersion relation, $n=\sigma T$ vs $q=kL$, for the RT instability in unbounded geometries. Here, $T=L^2/\sqrt{\nu D}$. The curves are numerical solutions of the eigenvalue problem for two different values of the Schmidt number, $S_C=\nu/D=500$ (full line) and 1000 (dashed line), and for a normalized mixing width $b=10$. The circles correspond to 2D lattice BGK simulations ($S_C=500$).

$$\frac{\partial\vec{V}}{\partial t}+\frac{6}{5}(\vec{V}\cdot\vec{\nabla})\vec{V}=-\frac{\vec{\nabla}P}{\rho}+\nu\Delta\vec{V}-\frac{\nu}{\kappa}\vec{V}+\vec{g}, \tag{8}$$

where $\kappa=h^2/12$ is the permeability and all vectors are two-dimensional. As the nonlinear term is negligible in our case, Eq. (8) leads to the unbounded geometry case for $1/\kappa\to 0$ (thick cells), and to the classical Darcy's law of a porous medium for $\kappa\to 0$ (thin cells).

We performed a linear stability analysis of Eq. (8) by working along the same lines as above, namely using a CDE, the Boussinesq approximation and a frozen-state approximation for the base-state concentration. It was found that it leads to the same normalized differential equation [Eq. (4)] and dispersion relations [Eqs. (6) and (7)], in the asymptotic regimes $b\to 0$ and $b\to\infty$, but now with

$$q_D^2=q^2+n\sqrt{S_C} \quad \text{and} \quad q_\nu^2=q^2+\frac{1}{K}+\frac{n}{\sqrt{S_C}}. \tag{9}$$

Here, the finite gap of the cell is contained in the normalized permeability K, which is proportional to the square of the ratio of the geometric length h and the fluid-dependent MRT length L: $K=\kappa/L^2=h^2/12L^2$.

Model 2. In a recent paper it was shown[9] that acceleration and viscous dissipation induce some departure of the gap velocity profile from the parabolic. The work in Ref. 9 accounts for first-order corrections to the Poiseuille flow, under small 2D acceleration and viscous dissipation. The resulting 2D equation reads as follows:

$$\frac{6}{5}\frac{\partial \vec{V}}{\partial t}+\frac{54}{35}(\vec{V}\cdot\vec{\nabla})\vec{V}=-\frac{\vec{\nabla}P}{\rho}+\frac{6}{5}\nu\Delta\vec{V}-\frac{\nu}{\kappa}\vec{V}+\vec{g}. \quad (10)$$

It is interesting to note that model 2 also leads to the correct porous media limit, $\kappa\to 0$ (long wave limit, LW), but does not allow to recover the Navier–Stokes equation for $1/\kappa\to 0$.

Clearly, the linear stability analysis of the RT problem on the basis of this equation will lead to a similar equation as before, with the exception of a correction factor 5/6. We find the equation

$$(q_D^2-d_{ZZ})(q_\nu^2-d_{ZZ})(q^2-d_{ZZ})W(Z)=\tfrac{5}{6}2q^2(dC/dZ)W(Z), \quad (11)$$

where

$$q_D^2=q^2+n\sqrt{S_C} \quad \text{and} \quad q_\nu^2=q^2+\frac{5}{6K}+\frac{n}{\sqrt{S_C}}. \quad (12)$$

The dispersion relations in the asymptotic limits $b\to 0$ and $b\to\infty$, respectively, are given by Eqs. (6) and (7), modified by the factor 5/6 on the right-hand side.

Stability predictions based on these two models will be compared below to the results of lattice BKG simulations. Before doing so, however, we also provide the corresponding stability calculations for an effective porous medium.

The Hele-Shaw cell geometry is often taken to model porous media flows. This analogy comes from the fact that the gap-averaged velocity (assuming a parabolic Poiseuille-like profile across the gap) leads to a 2D Darcy's law, where the 2D velocity is proportional to the pressure drop.[3] Displacements in porous media were addressed mainly in the context of viscous fingering; new phenomenology appears when viscosity and density contrasts act together.[2,10,11] In the present case of buoyancy instability without viscosity contrast, the pure porous medium case is obtained from Eqs. (4) and (9) of model 1 [or Eqs. (11) and (12) of model 2] in the limit $K\to 0$ (and under the assumption of a frozen base-state). We then obtain

$$(q_D^2-d_{ZZ})(q^2-d_{ZZ})W(Z)=2Kq^2\ (dC/dZ)W(Z). \quad (13)$$

For a step concentration profile, the dispersion relation and cutoff wave vector q_C are given by

$$(q_D+q)q_D=qK, \quad q_C=K/2 \quad (14)$$

and for a uniform density gradient, by

$$q_D^2=2K/\sqrt{\pi}B, \quad q_C^2=2K/\sqrt{\pi}b. \quad (15)$$

As Hele-Shaw cell experiments are routinely used to mimic porous media flows, it is of practical interest to delineate the range of physical parameters for which the porous media regime holds in the range of unstable wave lengths. As this regime is a LW approximation (i.e., $q^2K\ll 1$), the required condition is $q_C^2K\ll 1$, namely $K\ll 1$ and $K\ll\sqrt{b}$ in the limiting cases $b\ll 1$ and $b\gg 1$, respectively.

The results from the stability analyses of the various models were compared to lattice BGK simulations. We used models which are 2D with nine directions for the case of unbounded fluids, and 3D with 19 directions for the Hele-Shaw case,[5] and with periodic boundary conditions in the plane of the cell (x-direction). The equations simulated are the CDE of a tracer (the concentration of the mixture of the two miscible fluids) with a diffusion coefficient D, subject to the Navier–Stokes equations, with a kinematic viscosity ν. A body force proportional to the concentration is applied to model the gravity force under the Boussinesq approximation. Using as initial condition a frozen base state, where the concentration along the vertical direction z is steplike, or varies according to Eq. (2), we follow the time evolution, for $D=10^{-4}$ and $S_C=500$, of a sine perturbation of wavelength λ. In the 2D simulations we varied the normalized wave vector q by varying the characteristic length L (through the gravitational force), while keeping as constant the lattice size 256×64 and the wavelength $\lambda=64$. In the 3D simulations, the lateral dimension of the lattice (equal to λ) was varied from 24 to 264, and the choice of the normalized permeability, $K=1$ and 40.33, and of the gap thickness h (set to 7 and 44 for the smaller and the larger K, respectively) yielded a MRT length $L=h/\sqrt{12K}$ of the order of 2.

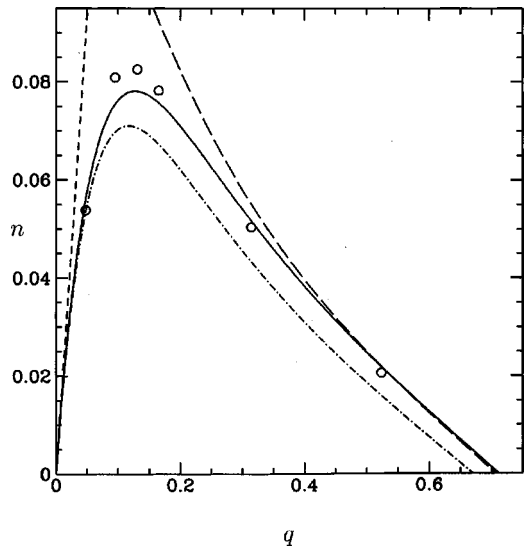

FIG. 2. Plot of the dispersion relation, n vs q, in a Hele-Shaw cell of dimensionless permeability $K=h^2/12L^2=40.33$, for $S_C=500$, $b=0$. Here, h is the gap thickness. The full line is the solution to the NSD equation (model 1), the dotted-dashed line is derived from the first order correction (Ref. 9) to the NSD (model 2), the short-dashed line corresponds to an effective porous medium [Eq. (14)], while the long-dashed line corresponds to the unbounded fluid case, modified to correct the wave number [Eq. (1)]. The circles are results of 3D lattice BGK simulations.

To compare the results of the different linear stability analyses with the 3D lattice BKG simulations, we first chose an intermediate regime between the effective porous medium and the unbounded medium regimes, namely a gap thickness h such that its permeability is $K=h^2/12L^2=40.33$, and a Schmidt number of $S_C=500$. Plotted in Fig. 2 are results corresponding to the step profile limit, $b=0$. The full line denotes the result from the analysis based on model 1, the dotted–dashed line corresponds to model 2, the short-dashed line corresponds to the porous medium case [Eq. (14)], while the long-dashed line is the 3D unbounded solution [Eq. (1)], modified to account for the wave vector in the gap of the cell (namely where k is replaced by $\sqrt{k^2-(\pi/h)^2}$). The open

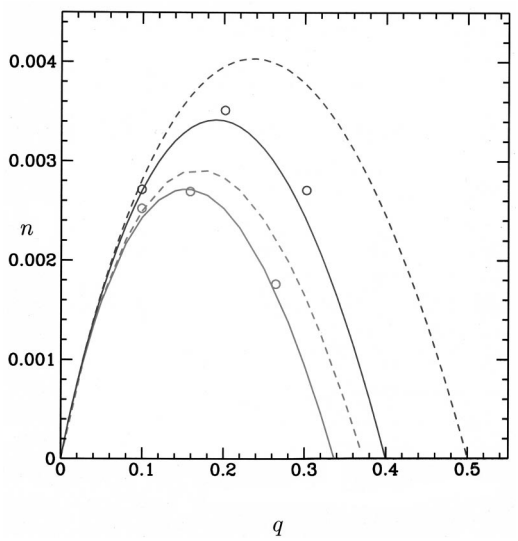

FIG. 3. Plot of the dispersion relation, n vs q, in a Hele-Shaw cell of dimensionless permeability $K=1$, for $S_C=500$, $b=0$ (upper two curves) and $b=\sqrt{12K}\sim 3.46$ (lower two curves). The latter case corresponds to $e=h$. The full lines are the solutions to the NSD equation (model 1) and the dashed lines correspond to an effective porous medium. The circles are results of 3D lattice BGK simulations.

circles in Fig. 2 correspond to the lattice BGK simulations.

Overall, the best agreement with the lattice BGK data is obtained by NSD model 1. Indeed, this model is closer to the 3D simulations, both in the vicinity of the maximum growth rate, as well as in that of the cutoff. In the LW limit, the best approximation to the data is given by NSD model 2, but we note that model 1 is also quite close. The unbounded geometry model, corrected for the wave number, compares well with the simulations in the short wave limit ($q^2K\gg 1$), but not in the long-wave limit. Conversely, the effective porous medium results approach the long-wave limit, but not the short-wave limit. In fact, the lattice BKG result for the smallest wave vector tried (for which $q^2K\sim 0.1$) already deviates from the porous media curve, although it does fall on the NSD model 2 curve.

Plotted in Fig. 3 are the results for a regime closer to the effective porous medium, namely $K=1$, and $b=0$ and $b=\sqrt{12}\sim 3.46$, which corresponds to a mixing length e equal to the gap size h. The full lines denote the result from the analysis based on model 1, the dashed lines correspond to the porous medium case, and the circles denote the results from the lattice BGK simulations. Note that the predictions of model 2 would be for these cases slightly below the curves given by model 1.

Figure 3 shows that the effective porous medium and NSD model 1 give very similar results at low wave vectors (typically $q<0.07$), but exhibit some discrepancies for the maximum growth rate n and the cutoff wave number q_C. Although n and q_C are larger for the porous medium case than for model 1, they both decrease when b increases. Overall, the NSD model 1 is closer to the 3D simulations.

Calculations (not displayed in the figure) show that the results of NSD model 1 and Darcy description fall on the same dispersion curves for $K\leqslant 0.2$. The value $K=0.2$ corresponds to a gap size h of the order of L. Simulations have not been performed in this range of K values, as they are more computing-time demanding (due to smaller growth rates and wave numbers), whereas the present 2D analyses are even more valid.

In conclusion, using the characteristic MRT length $L=(2\rho_0\nu D/\Delta\rho g)^{1/3}$ has allowed us to differentiate among the different regimes of the Rayleigh–Taylor instability of miscible fluids as a function of the confinement. In particular, the RT instability in a Hele-Shaw cell was found to be best described by the gap-averaged NSD model 1, which provides a correct approximation in the whole range of wave vectors, thus avoiding the need to handle the more complicated full 3D problem. We have also showed that the extension of the mixing zone comes into play when it is of the order or greater than L. Hele-Shaw cells can be used to mimic these instabilities in porous media, provided that the dimensionless permeability, K, and mixing width, b, fulfill the conditions $K\ll 1$ and $K\ll\sqrt{b}$ for $b\ll 1$ and $b\gg 1$, respectively. Outside this porous media regime, the 2D description (NSD, model 1) is necessary. Such a model is expected to also find applications in the context of chemical wave reaction-diffusion fronts in Hele-Shaw cells.[6]

ACKNOWLEDGMENTS

This Brief Communication benefited from discussions with Professor Y. C. Yortsos and Dr. C. Ruyer-Quil. This work was partly supported by IDRIS (Project No. 004052), CNES No. 793/CNES/00/8368, and ESA No. AO-99-083. All these sources of support are gratefully acknowledged.

[1] S. Chandrasekhar, *Hydrodynamic and Hydromagnetic Stability* (Oxford University Press, Oxford, 1961), and references therein.
[2] R. A. Wooding, "Growth of fingers at an unstable diffusing interface in a porous medium or Hele-Shaw cell," J. Fluid Mech. **39**, 477 (1969).
[3] R. A. Wooding, "Instability of a viscous liquid of variable density in a vertical Hele-Shaw cell," J. Fluid Mech. **7**, 501 (1960).
[4] G. K. Batchelor and J. M. Nitsche, "Instability of stationary unbounded stratified fluid," J. Fluid Mech. **227**, 357 (1991).
[5] N. Rakotomalala, D. Salin, and P. Watzky, "Miscible displacement between two parallel plates: BGK lattice gas simulations," J. Fluid Mech. **338**, 277 (1997); P. Gondret, N. Rakotomalala, M. Rabaud, D. Salin, and P. Watzky, "Viscous parallel flows in a finite aspect ratio Hele-Shaw cell: Analytical and numerical results," Phys. Fluids **9**, 1841 (1997).
[6] M. Böckmann and S. C. Müller, "Growth rate of the buoyancy-driven instability of an auto-catalytic reaction front in a narrow cell," Phys. Rev. Lett. **85**, 2506 (2000).
[7] P. Kurowski, C. Misbah, and S. Tchourkine, "Gravitational instability of a fictitious front during mixing of miscible fluids," Europhys. Lett. **29**, 309 (1995).
[8] C. Bizon, J. Werne, A. A. Predtechensky, K. Julien, W. D. McCormick, J. B. Swift, and H. L. Swinney, "Plume dynamics in quasi-2D turbulent convection," Chaos **7**, 107 (1997); P. Gondret and M. Rabaud, "Shear instability-fluid parallel flow in a Hele-Shaw cell," Phys. Fluids **9**, 3267 (1997).
[9] C. Ruyer-Quil, "Inertial corrections to the Darcy law in a Hele-Shaw cell," C. R. Acad. Sci., Ser. IIb: Mec., Phys., Chim., Astron. **329**, 337 (2001).
[10] J.-C. Bacri, D. Salin, and Y. C. Yortsos, "Analyse linéaire de la stabilité de l'écoulement de fluides miscibles en milieux poreux," C. R. Acad. Sci. Paris **314**, 139 (1992).
[11] O. Manickam and G. M. Homsy, "Fingering instabilities in vertical miscible displacement flows in porous media," J. Fluid Mech. **288**, 75 (1995).